Inorg. Chem. **2004**, *43*, 2427–2434

Crystal Structure and Magnetic Interactions in Nickel(II) Dibridged Complexes Formed by Two Azide Groups or by Both Phenolate Oxygen–Azide, –Thiocyanate, –Carboxylate, or –Cyanate Groups

Subrata Kumar Dey,[†] Nijhuma Mondal,[†] M. Salah El Fallah,*[,‡] Ramon Vicente,[‡] Albert Escuer,[‡] Xavier Solans,[‡] M. Font-Bardía,[‡] T. Matsushita,[§] V. Gramlich,[||] and Samiran Mitra*[,†]

Department of Chemistry, Jadavpur University, Kolkata-700 032, India, Departament de Química Inorgànica, Universitat de Barcelona, Martí i Franquès, 1-11, 08028-Barcelona, Spain, Department of Materials Chemistry, Faculty of Science and Technology, Ryukoku University, Seta, Otsu 520-2194, Japan, and Department of Chemistry, Laboratorium für Kristallographie ETH, Eidgenössische Technische Hochschule Zürich, CH-8092 Zürich, Switzerland

Received October 30, 2003

Tridentate/tetradentate Schiff base ligands L^1 and L^2, derived from the condensation of *o*-vanillin or pyridine-2-aldehyde with *N*,*N*-dimethylethylenediammine, react with nickel acetate or perchlorate salt and azide, cyanate, or thiocyanate to give rise to a series of dinuclear complexes of formulas $[Ni(L^1)(\mu_{1,1}\text{-}N_3)Ni(L^1)(N_3)(OH_2)]\cdot H_2O$ (**1**), $\{[Ni(L^1)(\mu_{1,1}\text{-}NCS)Ni(L^1)(NCS)(OH_2)][Ni(L^1)(\mu\text{-}CH_3COO)Ni(L^1)(\ NCS)\ (OH_2)]\}$ (**2**) {[**2A**][**2B**]}, $[Ni(L^1)(\mu_{1,1}\text{-}NCO)Ni(L^1)(NCO)(OH_2)]\cdot H_2O$ (**3**), and $[Ni(L^2\text{-}OMe)(\mu_{1,1}\text{-}N_3)(N_3)]_2$ (**4**), where $L^1 = Me_2N(CH_2)_2NCHC_6H_3(O^-)(OCH_3)$ and $L^2 = Me_2N(CH_2)_2NCHC_6H_3N$. We have characterized these complexes by analytical, spectroscopic, and variable-temperature magnetic susceptibility measurements. The coordination geometry around all of the Ni(II) centers is a distorted octahedron with bridging azide, thiocyanate/acetate, or cyanate in a $\mu_{1,1}$ mode and μ_2-phenolate oxygen ion for **1**–**3**, respectively, or with a double-bridging azide for **4**. The magnetic properties of the complexes were studied by magnetic susceptibility (χ_M) versus temperature measurements. The χ_M *vs T* plot reveals that compounds **1** and **4** are strongly ferromagnetically coupled, **3** shows a weak ferromagnetic behavior, and **2** is very weakly antiferromagnetically coupled.

Introduction

Binuclear metal complexes are effective devices for the recognition and assembly of external species. For this reason, the ligands obtained by forming binuclear complexes with various metal ions are of great interest. If the two metal ions are present in an unsaturated coordination environment, the binuclear complex can be used as a receptor for a secondary species. In this way, binuclear complexes mimic many biological sites, especially those in which the two metals can cooperate to form an active center as, for example, in oxygen receptors, activators, and carriers.[1] The nature of the two metal ions, their coordination requirements, and the distance between them are the key elements in assembling host species. Recent results from members of this group have demonstrated a thermally stable, Ni(III) complex bridged by an oxo group.[2] Exchange interactions propagated by discrete polyatomic bridging moieties (NCO, NCS, N_3, NCSe, etc.) between two paramagnetic centers have been the subject of several reviews[3,4] focusing on the ability of these pseudohalide ligands to coordinate with metals in a variety of ways. Many examples of azido-, thiocyanato-, and cyanato-bridged

* To whom correspondence should be addressed. E-mail: salah.elfallah@qi.ub.es (M.S.E.F.); smitra_2002@yahoo.com (S.M.). Fax: +91-33-2414-6266 (S.M.); +34 93 4907725 (M.S.E.F.).
[†] Jadavpur University.
[‡] Universitat de Barcelona.
[§] Ryukoku University.
[||] Eidgenössische Technische Hochschule.

(1) (a) Bianchi, A.; Bowman-James, K.; Garcia-España, E. *Supramolecular Chemistry of Anions*; Wiley-VCH: New York, 1997. (b) Martell, A. E.; Sawyer, D. T. *Oxygen Activation by Transition Metals*; Plenum Press: New York, 1987. (c) Lehn, J. M. *Supramolecular Chemistry. Concepts and Perspectives*; VCH: Weinheim, Germany, 1995.
(2) (a) Bag, B.; Mondal, N.; Rosiar, G.; Mitra, S. *J. Chem. Soc., Chem. Commun*. **2000**, 1729. (b) Burmeister, J. L. *Coord. Chem. Rev*. **1968,** *3*, 225.
(3) Norbury, A. H.; Sinha, A. I. P. *Q. Rev., Chem. Soc*. **1970**, *24*, 69.
(4) Kahn, O.; Pei, Y.; Journaux, Y. In *Inorganic Materials*, 2nd ed.; Bruce, Q. W., O'Hare, D., Eds.; J. Wiley: Chichester, U.K., 1997.

10.1021/ic0352553 CCC: $27.50
Published on Web 03/10/2004

compounds have been characterized.[5−16] In the case of nickel(II) ions, the structural and magnetic properties of octahedrally coordinated dimers with two pseudohalide bridging ligands have been studied.[17,18] One of the most appealing properties of binuclear transition metal complexes is the possible existence of exchange interactions between the metal centers. The design of molecule-based magnets relies on the presence of both intra- and intermolecular coupling. Therefore, the inspection of structural features, which correlate with strength and the sign of this interaction, clearly constitutes a necessary first step in this direction. Many structural parameters affect the superexchange mechanism in these sorts of dimers.[17,18] Kahn[19] has suggested that the exchange integral is the sum of two antagonistic interactions favoring the antiferromagnetic and ferromagnetic interactions. Bencini and Gatteschi[20] have shown, for end-to-end pseudohalide-bridged dimers, that antiferromagnetic contributions increase as the metal ion is moved out of the plane formed by the pseudohalide groups. The present paper deals with both the structural aspects and magnetic interactions of four nickel(II) dimers, where the metal atoms are dibridged by two azide groups or both the μ_2-phenolate oxygen atom and by azide, cyanate, thiocyanate, or acetate groups. Here, we report the crystal structures and magnetic properties of the complexes $[Ni(L^1)(\mu_{1,1}\text{-}N_3)Ni(L^1)(N_3)(OH_2)]\cdot H_2O$ (**1**), $\{[Ni(L^1)(\mu_{1,1}\text{-}NCS)Ni(L^1)(NCS)(OH_2)][Ni(L^1)(\mu\text{-}CH_3COO)Ni(L^1)(NCS)(OH_2)]\}$ (**2**) {[**2A**][**2B**]}, $[Ni(L^1)(\mu_{1,1}\text{-}NCO)Ni(L^1)(NCO)(OH_2)]\cdot H_2O$ (**3**), and $[Ni(L^2\text{-}OMe)(\mu_{1,1}\text{-}N_3)(N_3)]_2$ (**4**), where $L^1 = Me_2N(CH_2)_2NCHC_6H_3(O^-)(OCH_3)$ and $L^2 = Me_2N(CH_2)_2NCHC_6H_3N$.

Experimental Sections

Materials and Reagents. All chemicals were obtained from commercial sources and used as received. Solvents were purified, and $[Et_4N]ClO_4$ was prepared as previously reported.[21]

Spectral and Magnetic Measurements. Infrared spectra were recorded in KBr pellets using a Perkin-Elmer 883-IR spectrophotometer and on a Nicolet 520 FTIR spectrophotometer. Electronic spectra were recorded using a Perkin-Elmer λ-40 (UV−vis) spectrophotometer both in solution and in solid state (Nujol mull). Magnetic measurements on **1**−**3** were performed using a SQUID in the temperature range 300−2 K under an external magnetic field of 1000 G. The contribution of the sample holder was determined separately in the same temperature range and field. Magnetic measurements on complex **4** were performed using a DSM8 pendulum susceptometer, working in the temperature range 300−4 K. The applied external magnetic field was 1.5 T. Diamagnetic corrections were estimated from Pascal tables. EPR spectra were recorded using powder samples at X-band frequency with a Bruker 300E automatic spectrometer, varying the temperature between 4 and 300 K. The magnetic susceptibility was fitted by least-squares techniques. Elemental analyses (C, H, N) were performed on Perkin-Elmer 2400 II elemental analyzer. Cyclic voltammetric measurements of **1**−**3** were performed using an EG&G PARC electrochemical analysis system (model 250/5/0) under a dry nitrogen atmosphere using conventional, three-electrode configurations in purified acetonitrile with tetra-*n*-ethylammonium perchlorate as the supporting electrolyte. An ECDA-Pt02 platinum disk electrode produced from Con-Serv Enterprises, India, was used as the working electrode in cyclic voltammetry. Under the experimental conditions employed here, the ferrocene−ferrocenium couple appears at 0.47 V vs SCE (saturated calomel electrode) with a peak-to-peak separation of 70 mV at scan rate $\upsilon = 50$ mV s^{-1}. In the case of compound **4**, these measurements have not been possible due to low sample availability.

Synthesis of the Ligands. The Schiff bases L^1 and L^2 were prepared according to the procedure of Bharadwaj et al.[22a] for L^1 and by reflux of 2 mmol of pyridine-2-aldehyde and 2 mmol of *N*,*N*-dimethyl ethylenediamine in 10 mL of methanol for L^2 according to previously described methods.[22b]

Synthesis of the Complexes. $[Ni(L^1)(\mu_{1,1}\text{-}N_3)Ni(L^1)(N_3)(OH_2)]\cdot H_2O$ (1). Solid nickel acetate (0.248 g, 1 mmol) was added to a vigorously stirred 20 mL methanolic solution (1 mmol) of the ligand $[Me_2N(CH_2)_2NCHC_6H_3(OH)(OCH_3)]$, and an aqueous solution of NaN_3 (0.065 g, 1 mmol) was subsequently added with slow stirring. A green compound was obtained which was recrystallized from a 1:1 (v/v) methanol−dichloromethane solution. Shiny green, rectangular crystals were obtained after 2 days. Crystals were filtered out and air-dried. Yield: 57%.

Anal. Calcd for $Ni_2C_{24}H_{38}N_{10}O_6$: C,42.41; H, 5.44; N, 20.61; Ni, 17.28. Found: C, 42.5; H, 5.5; N, 20.6; Ni, 17.3.

IR: $\nu(N_3)$, 2055, 2036 cm^{-1}; ν(N−H), 3185−3330 cm^{-1}; $\nu(H_2O)$, 3406 cm^{-1}; ν(Ni−O) and ν(Ni−N), 463, 341, 277 cm^{-1}.

$[Ni(L^1)(\mu_{1,1}\text{-}CH_3COO)Ni(L^1)(NCS)][Ni(L^1)(\mu_{1,1}\text{-}NCS)Ni(L^1)(NCS)]$ (2) {[**2A**][**2B**]}**.** The procedure was the same as that for the dimer described above, except for the bridging ligand, an aqueous methanolic solution of NaNCS (0.081 g, 1 mmol) was added with slow stirring. Green, prismatic crystals were obtained after 10 days. Crystals were filtered out and air-dried. Yield: 77%.

Anal. Calcd for $Ni_4C_{53}H_{72}N_{11}O_{12}S_3$: C, 45.87; H, 5.19; N, 11.11; Ni, 16.94. Found: C, 46.0; H, 5.2; N, 11.1; Ni, 17.0.

IR (KBr): ν(NCS), 2125, 2089 cm^{-1}; ν_s(COO), 1659 cm^{-1}; ν_{as}(COO), 1386 cm^{-1}; ν(N−H), 3165−3350 cm^{-1}; $\nu(H_2O)$, 3420 cm^{-1}; ν(Ni−O) and ν(Ni−N), 469, 325, 269 cm^{-1}.

(5) Chaudhuri, P.; Weyhermüller, T.; Bill, E.; Weighardt, K. *Inorg. Chim. Acta* **1996**, *252*, 195.
(6) Vicente, R.; Escuer, A.; Ribas, J.; Solans, X. *Inorg. Chem*. **1992**, *31*, 1726.
(7) Escuer, A.; Vicente, R.; Ribas, J.; El Fallah, M. S.; Solans, X. *Inorg. Chem*. **1993**, *32*, 1033.
(8) Ribas, J.; Monfort, M.; Solans, X. Drillon, M. *Inorg. Chem*. **1994**, *33*, 742.
(9) Ruiz, E.; Cano, J.; Alvarez, S.; Alemany, P. *J. Am. Chem. Soc*. **1998**, *120*, 11122.
(10) Escuer, A.; Vicente, R.; Ribas, J.; El Fallah, M. S.; Solans, X.; Font-Bardía, M. *Inorg. Chem*. **1993**, *32*, 3727.
(11) Escuer, A.; Vicente, R.; Ribas, J.; El Fallah, M. S.; Solans, X.; Font-Bardía, M. *J. Chem. Soc., Dalton. Trans.* **1993**, 2975.
(12) Vicente, R.; Escuer, A.; Ribas, J.; Solans, X. *J. Chem. Soc., Dalton. Trans.* **1994**, 259.
(13) Monfort, M.; Bastos, C.; Diaz, C.; Ribas. J.; Solans, X. *Inorg. Chim. Acta* **1994**, *218*, 185.
(14) Escuer, A.; Vicente, R.; El Fallah, M. S.; Solans, X.; Font-Bardía, M. *J. Chem. Soc., Dalton. Trans.* **1996**, 1013.
(15) Duggan, D. M.; Hendrickson, D. N. *Inorg. Chem*. **1974**, *13*, 2056 and references therein.
(16) Landee, C. P.; Willlet, R. D. *Inorg. Chem*. **1981**, *20*, 2521.
(17) Ginsberg, A. P.; Martin, R. L.; Brookes, R. W.; Sherwood, R. C. *Inorg. Chem*. **1972**, *11*, 2884.
(18) Rojo, T.; Lezama, L.; Cortés, R.; Mesa, J. L.; Arriortua, M. I.; Villeneuve, G. *J. Magn. Mater*. **1990**, *83*, 519.
(19) Kahn, O. *Inorg. Chim. Acta* **1982**, *62*, 3.
(20) Bencini, A.; Gatteschi, D. *Inorg. Chim. Acta* **1978**, *31*, 11.
(21) Ray, M.; Ghosh, D.; Shirin, Z.; Mukherjee, R. *Inorg. Chem.* **1997**, *36*, 3568 and references therein.
(22) (a) Das, G.; Shukla, R.; Mandal, S.; Singh, R.; Bharadwaj, P. K.; Hall, J. V.; Whitmire, K. H. *Inorg. Chem*. **1997**, *36*, 323. (b) Zakrzewski, G.; Sacconi, L. *Inorg. Chem*. **1968**, *7*, 1034. Bamfield, P.; Price, R.; Miller, R. G. J. *J. Chem. Soc. A* **1969**, 1447.

Table 1. Crystal Data and Structure Refinement for Compounds **1**−**4**

	1	2	3	4
empirical formula	$C_{24}H_{38}N_{10}Ni_2O_6$	$C_{53}H_{72}N_{11}Ni_4O_{12}S_3$	$C_{26}H_{36}N_6Ni_2O_8$	$C_{22}H_{38}N_{18}Ni_2O_2$
fw	680.06	1386.24	678.03	704.12
temp (K)	293(2)	293(2)	293(2)	293(2)
wavelength (Å)	0.710 69	0.710 69	0.710 69	0.710 69
cryst system, space group	monoclinic, $P2_1/c$	monoclinic, $P2_1$	monoclinic, $P2_1/c$	triclinic, $P\bar{1}$
unit cell dimens (Å, deg)	$a = 16.100(12)$	$a = 13.8790(10)$	$a = 16.1420(10)$	$a = 10.111(3)$
	$b = 13.541(7)$	$b = 13.7700(10)$	$b = 13.6980(10)$	$b = 10.497(7)$
	$c = 13.929(9)$	$c = 16.3400(10)$	$c = 14.0200(10)$	$c = 16.695(18)$
	$\alpha = 90$	$\alpha = 90$	$\alpha = 90$	$\alpha = 73.73(7)$
	$\beta = 106.05(5)$	$\beta = 102.95$	$\beta = 104.740(10)$	$\beta = 84.58(4)$
	$\gamma = 90$	$\gamma = 90$	$\gamma = 90$	$\gamma = 67.73$
V (Å^3)	2918(3)	3043.4(4)	2998.0(4)	1574(2)
Z	4	2	4	2
d(calcd) (Mg/m^3)	1.548	1.513	1.502	1.486
abs coeff (mm^{-1})	1.347	1.389	1.313	1.250
cryst size (mm)	0.1 × 0.1 × 0.05	0.1 × 0.1 × 0.2	0.2 × 0.1 × 0.1	0.2 × 0.1 × 0.1
θ range for data collection (deg)	2.00−20.04	1.28−28.43	2.68−28.42	2.17−29.96
index ranges	$-15 \le h \le 14$, $-13 \le k \le 0$, $0 \le l \le 13$	$-18 \le h \le 17$, $0 \le k \le 18$, $0 \le l \le 21$	$-21 \le h \le 20$, $0 \le k \le 17$, $0 \le l \le 18$	$-14 \le h \le 14$, $-13 \le k \le 14$, $0 \le l \le 23$
reflns collected/unique	2889/2739 [R(int) = 0.0183]	6579/6579 [R(int) = 0.0000]	16838/6422 [R(int) = 0.0385]	9155/9152 [R(int) = 0.0274]
refinement method	full-matrix least squares on F^2	full-matrix least squares on F^2	full-matrix least squares on F^2	full-matrix least squares on F^2
data/restraints/params	2739/113/432	6579/7/742	6422/0/388	9105/0/449
goodness-of-fit on F^2	0.890	1.053	1.061	0.781
final R indices [$I > 2\sigma(I)$]	R1 = 0.0274, wR2 = 0.0616	R1 = 0.0296, wR2 = 0.0711	R1 = 0.0365, wR2 = 0.1016	R1 = 0.0370, wR2 = 0.0756
R indices (all data)	R1 = 0.0387, wR2 = 0.0633	R1 = 0.0539, wR2 = 0.0764	R1 = 0.0679, wR2 = 0.1092	R1 = 0.1308, wR2 = 0.1010
largest diff peak and hole (e Å^{-3})	0.464 and −0.322	0.309 and −0.267	1.466 and −0.329	0.960 and −0.495

Scheme 1

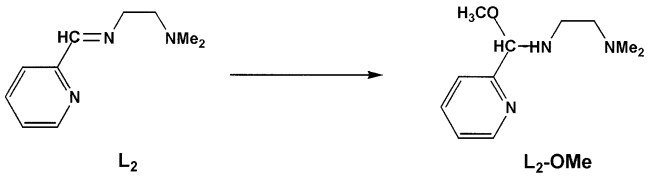

[Ni(L^1)($\mu_{1,1}$-NCO)Ni(L^1)(NCO)(OH$_2$)]·H$_2$O (3). The procedure was the same as that for the dimer described above, except for the bridging ligand, an aqueous solution of NaNCO (0.065 g, 1 mmol) was added with slow stirring. Green, prismatic crystals were obtained after 7 days. Crystals were filtered out and air-dried. Yield: 73%.

Anal. Calcd for $Ni_2C_{26}H_{36}N_6O_8$: C, 46.02; H, 5.31; N, 12.38; Ni, 17.31. Found: C, 46.1; H, 5.3; N, 12.4; Ni, 17.3.

IR: ν(NCO), 2210, 2201 cm^{-1}; ν(N−H), 3250−3329 cm^{-1}; ν(H$_2$O), 3415 cm^{-1}; ν(Ni−O) and ν(Ni−N), 458, 335, 279 cm^{-1}.

[Ni(L^2-OMe)$_2$($\mu_{1,1}$-N$_3$)(N$_3$)]$_2$ (4). A methanolic solution of 2 mmol of nickel perchlorate hexahydrate was added to a hot solution of the L^2 ligand in methanol. To a cold solution was added dropwise an aqueous, saturated solution of 4 mmol of sodium azide with continuous stirring. X-ray-quality, light green crystals of **4** were obtained by slow evaporation of the final solution. These crystals were unstable at room temperature and degraded within a few days but at −5 °C could be stored for months without quality loss.

Anal. Calcd for $Ni_2C_{22}H_{38}N_{18}O_2$: C, 37.53; H, 5.44; N, 35.80. Found: C, 37.9; H, 5.6; N, 35.4.

IR: ν(N$_3$), 2054, 2095 cm^{-1}; ν(N−H), 3300−3350 cm^{-1}.

During synthesis, the addition of one methanol molecule to the L^2 ligand (see Scheme 1) changed the sp^2 C and N atoms doubly bonded to sp^3 single bonded atoms.

X-ray Crystallography. Good quality crystals of compounds **1**−**4** were selected and mounted on a Syntex P2 diffractometer (**1**), a MAR345 diffractometer (**2** and **3**), or an ENRAF Nonius CAD4 four-circle diffractometer (**4**). The conditions for the intensity data collection and some features of the structural refinements are listed in Table 1. Graphite-monochromatized Mo Kα radiation (λ = 0.710 73 Å) and the ω scan technique were used to collect the data sets. A total of 2889 reflections (2739 independent reflections, R_{int} = 0.0183) for **1**, 6579 reflections (6579 independent reflections, R_{int} = 0.000) for **2**, 16 838 reflections (6422 independent reflections, R_{int} = 0.0385) for **3**, and 9155 reflections (9152 independent reflections, R_{int} = 0.027) for **4** were collected in the range $2° < \theta < 20.04°$ for **1**, $1.28° \le \theta \le 28.43°$ for **2**, $2.68° \le \theta \le 28.42°$ for **3**, and $2.17° \le \theta \le 29.96°$ for **4**, applying the condition $I > 2\sigma(I)$. The lattice constants were determined by least-squares refinements of the angular setting of 25 reflections near a θ value of 10°. The stability of the crystals was checked by measuring standard reflections at fixed intervals during the data collection. However, no significant loss of intensity was noted. The data were always corrected for Lorenz and polarization effects. The structure of **1** was solved by direct methods using the SHELXTL PLUS[23] system and refined by full-matrix least-squares methods based on F^2 using SHELXL93.[24] Structures **2** and **3** were solved by direct methods using the SHLEXS program[25] and refined by full-matrix, least-squares methods using the SHELX97 program.[26] Structure **4** was solved by direct methods using the SHELXS86 program[25] and refined by full-matrix, least-squares methods using the SHELX93 program.[24] The functions minimized were $\Sigma w[|F_o|^2 - |F_c|^2]^2$, where $w = [\sigma^2(I) + (0.0435P)^2]^{-1}$ for **1**, $[\sigma^2(I) + (0.0404P)^2 + 0.3220P]^{-1}$ for **2**, $[\sigma^2(I) + (0.0643P)^2]^{-1}$ for **3,** and $[\sigma^2(I) + (0.0484)^2]^{-1}$ for **4**, with $P = (|F_o|^2 + 2|F_c|^2)/3$. f, f', and f'' were taken from ref 27. All hydrogen atoms were computed and refined, using a riding model, with isotropic temperature factors equal to 1.2 times the equivalent temperature factor of the atom to which they are linked. The final R indices were 0.0274 for **1**, 0.0296 for **2**, 0.0365 for **3**, and 0.0370 for **4**, respectively, for all observed reflections.

(23) Sheldrick, G. M. *SHELXL-PLUS*; Siemens X-ray Analytical Instruments Inc.: Madison, WI, 1990.
(24) Sheldrick, G. M. *SHELXL 93: Computer Program for Crystal Structure Refinement*; Universität Göttingen: Göttingen, Germany, 1993.
(25) Sheldrick, G. M. *Computer Program for Determination of Crystal Structure*; Universität Göttingen: Göttingen, Germany, 1997. Sheldrick, G. M. *SHELXS-86, Program for the Solution of Crystal Structure*; Universität Göttingen: Göttingen, Germany, 1986.
(26) Sheldrick, G. M. *SHELXL-97, Computer Program for the refinement of Crystal Structure*; Universität Göttingen: Göttingen, Germany, 1997.
(27) *International Tables for X-ray Crystallography*; Kynoch Press: Birmingham, U.K., 1974; Vol. IV, pp 99−101, 149.

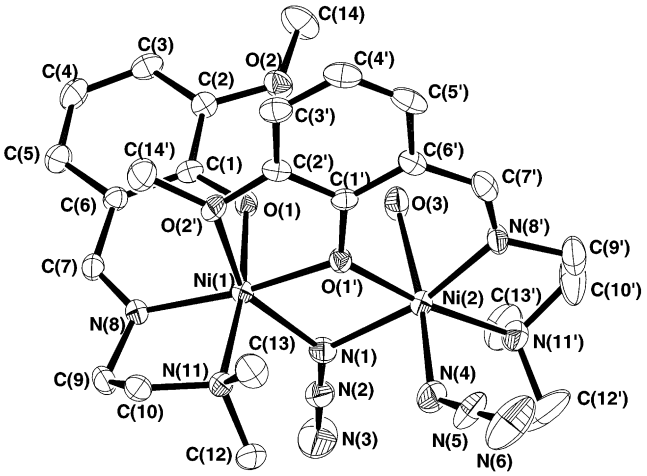

Figure 1. ORTEP drawing of complex **1** showing the atom labeling scheme.

Maximum and minimum peaks (e A^{-3}) in the final difference Fourier synthesis were 0.464 and −0.322 for **1**, 0.309 and − 0.267 for **2**, 1.466 and −0.329 for **3**, and 0.960 and −0.495 for **4**, respectively.

Results and Discussion

Description of the Structures of 1−3. The structures of **1**−**3** are based on the same Schiff base ligand but with different bridging ligands: N_3^- in **1**; OCN^- in **3**; SCN^- and $CH_3CO_2^-$ in **2A**,**B**, respectively. In the present complexes, the two Schiff base molecules behave differently. One of the two Schiff bases acts as a tetradentate molecule, while the other acts in a tridentate fashion with a nonbonded methoxy group. Generally, the structural trends of **1**, **2A**, **B**, and **3** are similar, except for a slight difference in the bond parameters and the standard deviations. We, therefore limit detailed description to the structure of **1**, highlighting only the important differences in the case of the other structures, and later we will concentrate on the description of the structure of **4**.

The molecular structure of **1** is shown in Figure 1. The selected bond lengths and bond angles are summarized in Table 2. The dinuclear unit is formed by two Ni(II) atoms labeled Ni(1) and Ni(2), bridged by one azide group in end-on fashion through N(1) and by μ_2-phenolate oxygen atom O(1′) of the Schiff base. The coordination sites of the octahedral Ni(1) atom are completed by two nitrogen N(8) and N(11) and one oxygen O(1) of the same Schiff base ligand and by a methoxy oxygen atom O(2′) of the bridging phenolic moiety. Similarly, the remaining sites of distorted octahedral geometry of Ni(2) atom are occupied by one nitrogen atom N(4) of a free azide ligand and two nitrogen atoms N(8′) and N(11′) of the Schiff base and by the coordinated oxygen atom O(3) of a water molecule. Deviation of the Ni(1) and Ni(2) atoms from the mean plane formed by the two nitrogens and two oxygens of Ni(1) and by three nitrogens and one oxygen of Ni(2) are 0.030 and 0.098 Å, respectively. The basal bond distances around the Ni(1) atom are in the 2.264−1.984 Å range. The apical bond distances are Ni(1)−N(11) = 2.155(3) Å and Ni(1)−O(1) = 1.996(2) Å considering the bond angle O(1)−Ni(1)−N(11) = 171.66(10)°. The other bond distances are Ni(1)−N(8) = 1.984(3) Å, Ni(1)−N(1) = 2.146(3) Å, Ni(1)−O(1′) = 1.989(2) Å, and Ni(1)−O(2′) = 2.264(3) Å. The bond distances around the Ni(2) atom are in the 2.211−1.984 Å range. The apical bond distances are Ni(2)−N(4) = 2.057(3) Å and Ni(2)−O(3) = 2.211(3) Å considering the bond angle N(4)−Ni(2)−O(3) = 173.80(11)°. The other bond distances are Ni(2)−N(8′) = 1.998(3) Å, Ni(2)−N(11′) = 2.140(3) Å, Ni(2)−O(1′) = 1.984(2) Å, and Ni(2)−N(1) = 2.127(3) Å. The major distortion from a "regular" octahedron for two nickel centers could be a result of the coordination of one free azide and one coordinated hydroxyl group around the Ni(2) center and the μ_2 bridging of the phenolate group. The largest bond between Ni(1) and O(2′) is most probably due to the bonding of the phenolate oxygen atom of the same ring and to the coordination of hydroxyl group. One elongated Ni(2)−O(3) bond is present, which is weakly held and is responsible for the deviation from actual octahedral geometry which is also evident from N(4)−Ni(2)−O(3) bond angle.

Table 2. Selected Bond Lengths (Å) and Angles (deg) for Compound **1**

Ni(1)−N(8)	1.984(3)	Ni(1)−O(1′)	1.989(2)
Ni(1)−O(1)	1.996(2)	Ni(1)−N(1)	2.146(3)
Ni(1)−N(11)	2.155(3)	Ni(1)−O(2′)	2.264(3)
Ni(2)−O(1′)	1.984(2)	Ni(2)−N(8′)	1.998(3)
Ni(2)−N(4)	2.057(3)	Ni(2)−N(1)	2.127(3)
Ni(2)−N(11′)	2.140(3)	Ni(2)−O(3)	2.211(3)
O(1)−Ni(1)−N(11)	171.66(10)	N(4)−Ni(2)−O(3)	173.80(11)
Ni(1)−O(1′)−Ni(2)	106.83(10)	Ni(1)−N(1)−Ni(3)	96.62(10)
N(8)−Ni(1)−O(1′)	169.92(10)	N(8)−Ni(1)−O(1)	90.00(11)
O(1)−Ni(1)−O(1′)	90.01(10)	N(8)−Ni(1)−N(1)	112.12(12)
O(1′)−Ni(1)−N(1)	77.96(11)	O(1)−Ni(1)−N(1)	89.69(11)
N(8)−Ni(1)−N(11)	82.58(12)	O(1′)−Ni(1)−N(11)	96.61(11)
N(1)−Ni(1)−N(11)	96.62(12)	N(11′)−Ni(2)−O(3)	92.37(11)
N(8)−Ni(1)−O(2′)	96.04(11)	O(1′)−Ni(1)−O(2′)	73.90(10)
O(1)−Ni(1)−O(2′)	86.97(10)	N(1)−Ni(1)−O(2′)	151.65(10)
N(11)−Ni(1)−O(2′)	90.00(11)	O(1′)−Ni(2)−N(8′)	89.79(12)
O(1′)−Ni(2)−N(4)	91.90(13)	N(8′)−Ni(2)−N(4)	96.61(14)
O(1′)−Ni(2)−N(1)	78.51(11)	N(8′)−Ni(2)−N(1)	166.75(12)
N(4)−Ni(2)−N(1)	90.02(13)	O(1′)−Ni(2)−N(11′)	172.68(11)
N(8′)−Ni(2)−N(11′)	84.01(13)	N(4)−Ni(2)−N(11′)	92.67(13)
N(1)−Ni(2)−N(11′)	107.19(13)	O(1′)−Ni(2)−O(3)	83.45(10)
N(8′)−Ni(2)−O(3)	87.50(11)	N(1)−Ni(2)−O(3)	85.04(11)

The two independent binuclear units [Ni(L^1)($\mu_{1,1}$-NCS)-Ni(L^1)(NCS)(OH_2)] (**2A**) and [Ni(L^1)(μ-CH_3COO)Ni(L^1)-(NCS)(OH_2)] (**2B**) (L^1 = $Me_2N(CH_2)_2NCHC_6H_3(O^-)(OCH_3)$) which form the asymmetric unit of **2** are shown in Figure 2. In the unit **2A** there are two similar pseudooctahedral Ni(II) centers, one with a N_4O_2 donor set for Ni(1) and another with a N_3O_3 donor set for Ni(2), which are held together by both an isothiocyanate group in $\mu_{1,1}$ end-on fashion via a nitrogen atom and the μ_2-phenolate oxygen atom of a Schiff base ligand. Here, two Schiff base molecules behave differently. The Ni(1)···Ni(2) distance is 3.328(4) Å and Ni(1)−O(1)−Ni(2) and Ni(1)−N(31)−Ni(2) angles are 110.5(2) and 96.63(17)°, respectively, while in the unit **2B** the two pseudooctahedral Ni(3) and Ni(4), with a N_2O_4 donor set and a N_3O_3 donor set, respectively, are bridged by both the acetate ligand in *syn*−*syn* fashion and the μ_2-phenolate oxygen atom of a Schiff base ligand. The Ni(3)···Ni(4) distance is 3.344(4) Å, and Ni(3)−O(3A)−Ni(4) angle is

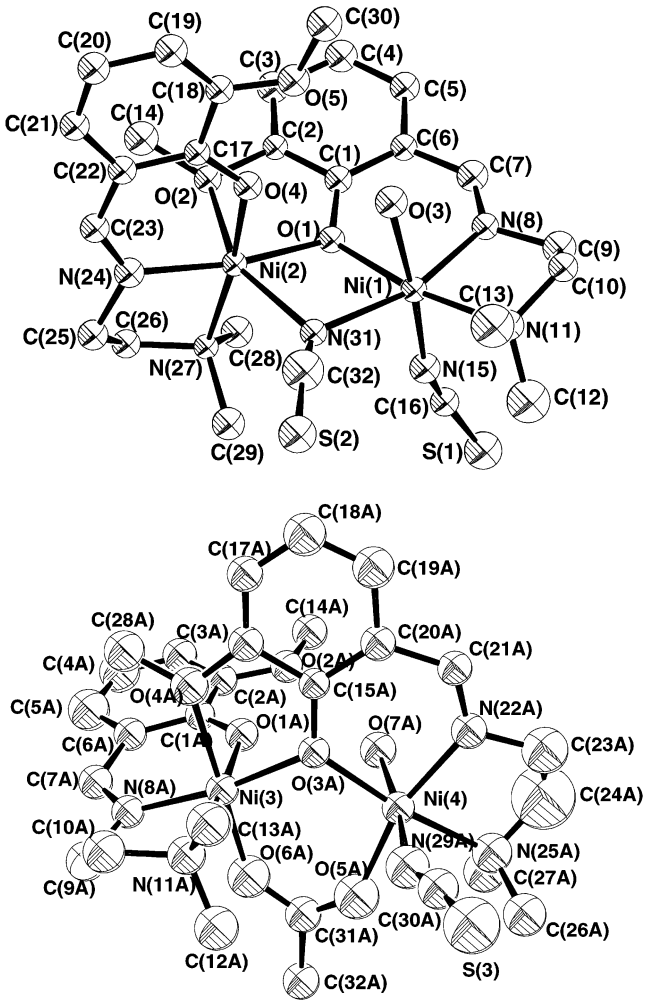

Figure 2. ORTEP drawing of complex **2** showing the atom labeling scheme.

112.3(2)°. The important bond lengths and bond angles of **2** are summarized in Table 3.

The structure of complex **3** is isostructural to that described above for complex **1**, except that it contains a OCN^- anion instead of the N_3^- anion in **1**. In the present case the Ni··· Ni distance is 3.305(3) Å and the Ni(1)−O(6)−Ni(2) and Ni(1)−N(1)−Ni(2) angles are 110.44(7) and 96.20(14)°. The ortep drawing of the structure is shown in Figure 3, and the important bond lengths and angles are summarized in Table 4.

Description of the Structure 4. The structure of **4** consists of neutral, well-isolated dinuclear $[Ni_2(L^2\text{-}OMe)_2(N_3)_4]$ units. A view of a dinuclear unit with the atom-labeling scheme is shown in Figure 4. Selected bond lengths and angles are shown in Table 5. The two nickel centers of the dinuclear unit have different bond parameters, but they are placed in a distorted octahedral environment formed by the three N atoms of the L^2-OMe ligand, one N atom of one terminal azido ligand, and the two N atoms of two azido ligands which act as a bridge between the two nickel atoms in the end-on coordination mode. The sp^3 hybridization of the C(6) and C(18) atoms allows the *fac* coordination of L^2-OMe in contrast to the planar rigid Schiff base L^2. The bond distances around the nickel atoms are very small, in the range Ni(1)−

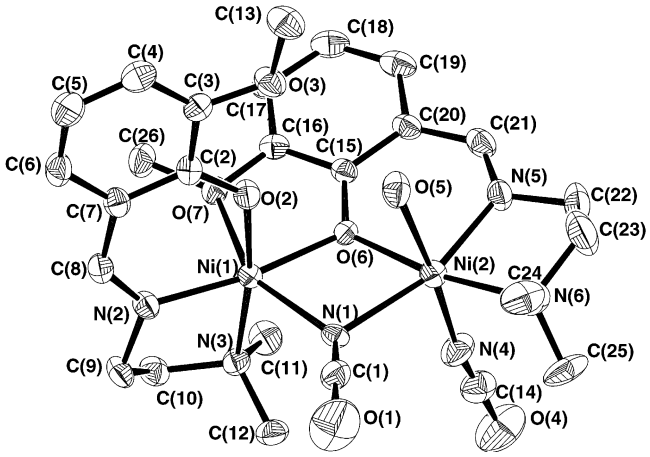

Figure 3. ORTEP drawing of complex **3** showing the atom labeling scheme.

Table 3. Selected Bond Lengths (Å) and Angles (deg) for Compound **2**

Ni(1)−N(8)	1.969(5)	Ni(1)−N(15)	2.041(7)
Ni(1)−O(1)	2.048(5)	Ni(1)−N(11)	2.166(5)
Ni(1)−N(31)	2.207(4)	Ni(1)−O(3)	2.209(5)
Ni(2)−O(4)	1.988(4)	Ni(2)−O(1)	2.003(4)
Ni(2)−N(24)	2.005(6)	Ni(2)−N(27)	2.169(5)
Ni(2)−O(2)	2.225(4)	Ni(2)−N(31)	2.250(5)
Ni(4)−O(3A)	2.015(4)	Ni(4)−O(5A)	2.026(3)
Ni(4)−N(22A)	2.044(5)	Ni(4)−N(29A)	2.055(7)
Ni(4)−O(7A)	2.158(4)	Ni(4)−N(25A)	2.184(6)
Ni(3)−N(8A)	1.968(5)	Ni(3)−O(1A)	2.008(4)
Ni(3)−O(3A)	2.011(4)	Ni(3)−O(6A)	2.047(3)
Ni(3)−N(11A)	2.181(5)	Ni(3)−O(4A)	2.235(5)
Ni(1)−(O1)−Ni(2)	110.5(2)	Ni(1)−N(31)−Ni(2)	96.6(2)
N(8)−Ni(1)−N(15)	91.7(2)	N(8)−Ni(1)−O(1)	89.56(19)
N(15)−Ni(1)−O(1)	92.03(19)	N(8)−Ni(1)−N(11)	83.2(2)
N(15)−Ni(1)−N(11)	94.0(2)	O(1)−Ni(1)−N(11)	170.7(2)
N(8)−Ni(1)−N(31)	163.4(2)	N(15)−Ni(1)−N(31)	97.4(2)
O(1)−Ni(1)−N(31)	76.29(16)	N(11)−Ni(1)−N(31)	109.9(2)
N(8)−Ni(1)−O(3)	89.7(2)	N(15)−Ni(1)−O(3)	174.3(2)
O(1)−Ni(1)−O(3)	82.46(18)	N(11)−Ni(1)−O(3)	91.7(2)
N(31)−Ni(1)−O(3)	79.90(17)	O(4)−Ni(2)−O(1)	90.26(17)
O(4)−Ni(2)−N(24)	89.7(2)	O(1)−Ni(2)−N(24)	168.1(2)
O(4)−Ni(2)−N(27)	173.27(19)	O(1)−Ni(2)−N(27)	95.66(17)
N(24)−Ni(2)−N(27)	83.8(2)	O(4)−Ni(2)−O(2)	89.23(19)
O(1)−Ni(2)−O(2)	76.38(17)	N(24)−Ni(2)−O(2)	91.7(2)
N(27)−Ni(2)−O(2)	89.03(17)	O(4)−Ni(2)−N(31)	88.44(18)
O(1)−Ni(2)−N(31)	76.19(17)	N(24)−Ni(2)−N(31)	115.7(2)
N(27)−Ni(2)−N(31)	96.09(17)	O(2)−Ni(2)−N(31)	152.45(16)
O(3A)−Ni(4)−O(5A)	105.18(17)	O(3A)−Ni(4)−N(22A)	91.2(2)
O(5A)−Ni(4)−N(22A)	163.5(2)	O(3A)−Ni(4)−N(29A)	91.0(2)
O(5A)−Ni(4)−N(29A)	85.3(2)	N(22A)−Ni(4)−N(29A)	92.3(2)
O(3A)−Ni(4)−O(7A)	83.55(16)	O(5A)−Ni(4)−O(7A)	93.40(18)
N(22A)−Ni(4)−O(7A)	90.52(19)	N(29A)−Ni(4)−O(7A)	173.9(2)
O(3A)−Ni(4)−N(25A)	172.16(19)	O(5A)−Ni(4)−N(25A)	80.9(2)
N(22A)−Ni(4)−N(25A)	83.0(2)	N(29A)−Ni(4)−N(25A)	94.4(2)
O(7A)−Ni(4)−N(25A)	91.26(19)	N(8A)−Ni(3)−O(1A)	91.1(2)
N(8A)−Ni(3)−O(3A)	170.52(19)	O(1A)−Ni(3)−O(3A)	88.92(17)
N(8A)−Ni(3)−O(6A)	83.37(18)	O(1A)−Ni(3)−O(6A)	88.49(17)
O(3A)−Ni(3)−O(6A)	106.10(16)	N(8A)−Ni(3)−N(11A)	82.7(2)
O(1A)−Ni(3)−N(11A)	173.7(2)	O(3A)−Ni(3)−N(11A)	97.11(19)
O(6A)−Ni(3)−N(11A)	91.59(19)	N(8A)−Ni(3)−O(4A)	94.8(2)
O(1A)−Ni(3)−O(4A)	87.88(18)	O(3A)−Ni(3)−O(4A)	75.69(17)
O(6A)−Ni(3)−O(4A)	175.93(18)	N(11A)−Ni(3)−O(4A)	91.81(19)
Ni(3)−O(3A)−Ni(4)	112.35(18)		

N(7) = 2.040(3), Ni(1)−N(4) = 2.144(3) Å for Ni(1) and Ni(2)−N(1) = 2.082(3), Ni(2)−N(4) = 2.166(2) Å for Ni(2). The central $Ni(N_3)_2Ni$ ring is slightly distorted by planarity (torsion Ni(1)−N(1)−Ni(2)−N(4) of 9.1°) and quite asymmetric, showing Ni(1)−N(1) = 2.131(2), Ni(1)−N(4) = 2.144(3), Ni(2)−N(1) = 2.082(3), and Ni(2)−N(4) =

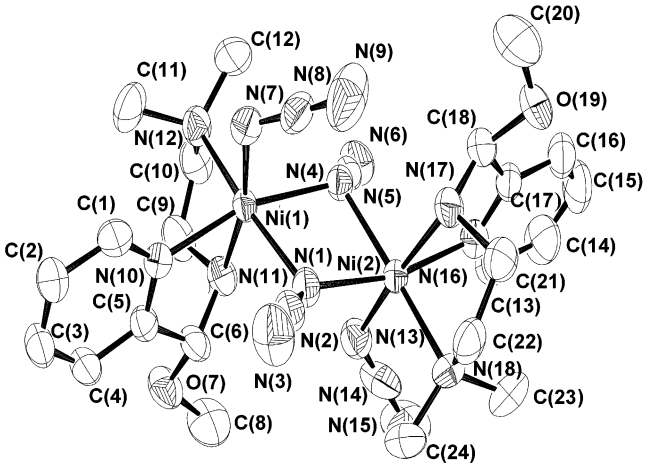

Figure 4. ORTEP drawing of complex **4** showing the atom labeling scheme.

Table 4. Selected Bond Lengths (Å) and Angles (deg) for Compound **3**

Ni(1)−N(2)	1.9932(19)	Ni(1)−O(2)	2.0003(16)
Ni(1)−O(6)	2.0079(15)	Ni(1)−N(1)	2.015(4)
Ni(1)−N(3)	2.1783(19)	Ni(1)−N(1)	2.203(4)
Ni(1)−O(7)	2.2351(17)	Ni(2)−O(6)	2.0165(16)
Ni(2)−N(4)	2.020(2)	Ni(2)−N(5)	2.021(2)
Ni(2)−N(6)	2.172(3)	Ni(2)−O(5)	2.2313(19)
Ni(2)−N(1)	2.238(4)		
Ni(1)−O(6)−Ni(2)	110.44(8)	Ni(1)−N(1)−Ni(2)	96.19(6)
N(2)−Ni(1)−O(6)	169.45(8)	O(2)−Ni(1)−O(6)	88.89(7)
N(2)−Ni(1)−N(1)	83.13(14)	O(2)−Ni(1)−N(1)	89.42(15)
O(6)−Ni(1)−N(1)	107.37(13)	N(2)−Ni(1)−N(3)	82.60(8)
O(2)−Ni(1)−N(3)	171.84(7)	O(6)−Ni(1)−N(3)	97.37(7)
N(1)−Ni(1)−N(3)	93.67(14)	N(2)−Ni(1)−N(1)	113.50(11)
O(2)−Ni(1)−N(1)	90.71(11)	O(6)−Ni(1)−N(1)	77.03(11)
N(1)−Ni(1)−N(1)	30.40(15)	N(3)−Ni(1)−N(1)	95.78(11)
N(2)−Ni(1)−O(7)	94.13(7)	O(2)−Ni(1)−O(7)	87.37(7)
O(6)−Ni(1)−O(7)	75.33(6)	N(1)−Ni(1)−O(7)	175.77(15)
N(3)−Ni(1)−O(7)	89.16(7)	N(1)−Ni(1)−O(7)	152.33(11)
O(6)−Ni(2)−N(4)	93.14(9)	O(6)−Ni(2)−N(5)	90.02(8)
N(4)−Ni(2)−N(5)	93.56(10)	O(6)−Ni(2)−N(6)	170.39(8)
N(4)−Ni(2)−N(6)	93.68(11)	N(5)−Ni(2)−N(6)	82.80(10)
O(6)−Ni(2)−O(5)	82.16(7)	N(4)−Ni(2)−O(5)	174.95(9)
N(5)−Ni(2)−O(5)	88.32(8)	N(6)−Ni(2)−O(5)	91.21(9)
O(6)−Ni(2)−N(1)	76.06(11)	N(4)−Ni(2)−N(1)	95.65(13)
N(5)−Ni(2)−N(1)	163.68(12)	N(6)−Ni(2)−N(1)	109.96(13)
O(5)−Ni(2)−N(1)	81.46(11)		

2.166(2) Å bond distances and Ni(1)−N(1)−Ni(2) = 102.5(1) and Ni(1)−N(4)−Ni(2) = 99.4(1)° bond angles.

An analysis performed using the CSD revealed that the distances Ni···Ni, Ni···O, and Ni···N for all the complexes are comparable to those of the previously reported similar Ni(II) complexes.[28]

Electronic Spectra. The peaks in the electronic spectrum of each of the complexes, both in the solid state (Nujol mull) and in acetonitrile solution, are similar, exhibiting d−d maxima typical of octahedral Ni^{II}.[22] The bands at λ_{max} values of 605−619, 627−642, and 386−347 nm regions are assigned to the spin-allowed transitions $^3T_{1g} \leftarrow {}^3A_{2g}$ and $^3T_{1g}(P) \leftarrow {}^3A_{2g}$, respectively, under O_h symmetry. The shoulder at around 721−730 nm originates from the spin-forbidden $^1E_g \leftarrow {}^3A_{2g}$ transition frequently observed in Ni(II) octahedral complexes. The appearance of two bands in the region of the $^3T_{1g}(P) \leftarrow {}^3A_{2g}$ transition reflects the different chromophores and may suggest a lower symmetry (D_{4h}).

Table 5. Selected Bond Lengths (Å) and Angles (deg) for Compound **4**

Ni(1)−N(1)	2.131(2)	Ni(2)−N(1)	2.082(3)
Ni(1)−N(4)	2.144(3)	Ni(2)−N(4)	2.166(2)
Ni(1)−N(7)	2.040(3)	Ni(2)−N(13)	2.086(4)
Ni(1)−N(10)	2.093(3)	Ni(2)−N(16)	2.099(3)
Ni(1)−N(11)	2.110(3)	Ni(2)−N(17)	2.139(3)
Ni(1)−N(12)	2.144(2)	Ni(2)−N(18)	2.155(2)
N(1)−N(2)	1.208(3)	N(7)−N(8)	1.164(3)
N(2)−N(3)	1.135(4)	N(8)−N(9)	1.166(4)
N(4)−N(5)	1.207(3)	N(13)−N(14)	1.112(4)
N(5)−N(6)	1.147(3)	N(14)−N(15)	1.189(4)
N(1)−Ni(1)−N(4)	78.06(9)	N(1)−Ni(2)−N(4)	78.6(1)
N(1)−Ni(1)−N(7)	93.4(1)	N(1)−Ni(2)−N(13)	90.7(1)
N(1)−Ni(1)−N(10)	88.66(9)	N(1)−Ni(2)−N(16)	165.9(1)
N(1)−Ni(1)−N(11)	94.9(1)	N(1)−Ni(2)−N(17)	95.1(1)
N(1)−Ni(1)−N(12)	172.66(9)	N(1)−Ni(2)−N(18)	95.5(1)
N(4)−Ni(1)−N(7)	97.6(1)	N(4)−Ni(2)−N(13)	89.2(1)
N(4)−Ni(1)−N(10)	163.57(9)	N(4)−Ni(2)−N(16)	88.9(1)
N(4)−Ni(1)−N(11)	92.9(1)	N(4)−Ni(2)−N(17)	92.8(1)
N(4)−Ni(1)−N(12)	94.9(1)	N(4)−Ni(2)−N(18)	172.5(1)
N(7)−Ni(1)−N(10)	92.8(1)	N(13)−Ni(2)−N(16)	95.8(1)
N(7)−Ni(1)−N(11)	167.8(1)	N(13)−Ni(2)−N(17)	174.1(1)
N(7)−Ni(1)−N(12)	89.6(1)	N(13)−Ni(2)−N(18)	95.5(1)
N(10)−Ni(1)−N(11)	78.5(1)	N(16)−Ni(2)−N(17)	79.0(1)
N(10)−Ni(1)−N(12)	97.9(1)	N(16)−Ni(2)−N(18)	96.4(1)
N(11)−Ni(1)−N(12)	83.3(1)	N(17)−Ni(2)−N(18)	83.1(1)
Ni(1)−N(1)−Ni(2)	102.54(11)	Ni(1)−N(4)−Ni(2)	99.38(10)
N(2)−N(1)−Ni(2)	134.35(19)	N(5)−N(4)−Ni(2)	113.82(19)
N(14)−N(13)−Ni(2)	126.9(3)	N(2)−N(1)−Ni(1)	118.86(19)
N(5)−N(4)−Ni(1)	124.96(18)	N(8)−N(7)−Ni(1)	122.4(2)
N(3)−N(2)−N(1)	179.6(3)	N(6)−N(5)−N(4)	178.7(3)
N(7)−N(8)−N(9)	176.6(3)	N(13)−N(14)−N(15)	179.3(4)

Cyclic Voltammetry of Nickel(II) Complexes. The electrochemical behavior of the complex **1** has been essayed by cyclic voltammetry in acetonitrile solution under a N_2 atmosphere to investigate the extent of stabilization of Ni(II) state toward oxidation. A CV scan of **1** in acetonitrile at a platinum electrode shows one irreversible Ni(III/II)couple at $E_{1/2} = 0.72$ V vs SCE with ΔE_p value of 200 mV, which suggests that the Ni(III) species is unstable and undergoes speedy decomposition.

CV studies on complexes **2** and **3** in acetonitrile at a platinum electrode demonstrate behavior identical with that observed for complex **1**. The $E_{1/2}$ values for complexes **2** and **3** are 0.66 and 0.56 V vs SCE with ΔE_p values of 338 and 586 mV, respectively.

Magnetic Study. Compounds **1** and **4** are strongly ferromagnetically coupled, while compound **3** shows a weak ferromagnetic behavior. Plots of $\chi_M T$ vs T for **1**, **4** (Figure 5), and **3** (Figure 6) show typical ferromagnetic behaviors: an increase in the effective magnetic moment with decreasing temperature. At 300 K $\chi_M T$ values are 2.60, 2.85, and 2.42 cm^3 K mol^{-1} for **1**, **4**, and **3**, respectively. This quantity increases up to maximum values of 3.42 cm^3 K mol^{-1} at 20 K for **1**, 3.75 cm^3 K mol^{-1} at 24 K for **4**, and 2.52 cm^3 K mol^{-1} at 17 K for **3**. Below this temperature, $\chi_M T$ decreases gradually due to ZFS of ground state ($S = 2$) or due to possible interactions between the dimers, reaching values of 2.72 cm^3 K mol^{-1} for **1**, 2.80 cm^3 K mol^{-1} for **4**, and 1.19 cm^3 K mol^{-1} for **3** at 2 K.

The $\chi_M T$ vs temperature curves for **1**, **4**, and **3** were least-squares fitted (by minimizing the function $R = \Sigma[(\chi_M T)_{exp}$

(28) Allen, F. H.; Kennard, O. Cambridge Structural Database. *Chem. Des. Autom. News* **1993**, *8*, 31.

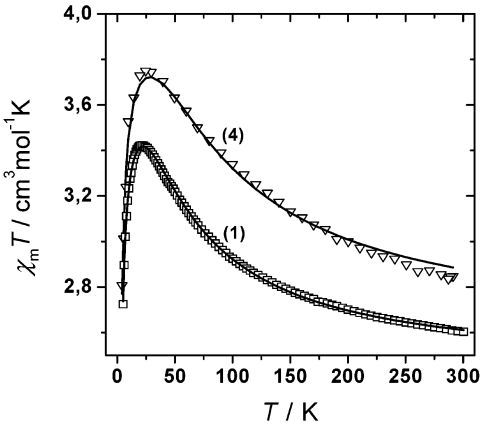

Figure 5. Experimental and calculated (solid line) temperature dependence of $\chi_M T$ for **1** and **4**.

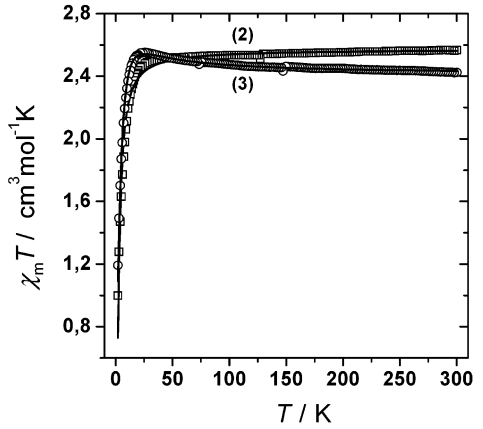

Figure 6. Experimental and calculated (solid line) temperature dependence of $\chi_M T$ for **2** and **3**.

$-(\chi_M T)_{cal}]^2/\Sigma(\chi_M T)_{exp}^2)$ to the theoretical expression of the magnetic susceptibility of Ginsberg et al.,[29−31] from the Hamiltonian

$$H = -2JS_1S_2 - D(S_{1Z}{}^2 + S_{2Z}{}^2) - g\beta H(S_1 + S_2) - Z'J'S\langle S\rangle$$

in which J is the intradimer exchange parameter, D the single-ion zero-field splitting, and $Z'J'$ the quantity for effective interdimer exchange; it is assumed that $g_x = g_y = g_z = g$. The resulting χ_M expression is

$$\chi_M = 2Ng^2\beta^2/3k[F_1/(T - 4Z'J'F_1) + 2F'/(1 - 4Z'J'F')]$$

F_1 and F' being complicated functions of temperature, zero-field splitting, and the intradimer exchange parameter J.

The best-fitting parameters obtained are $J = +25.6$ cm^{-1}, $g = 2.20$, $D = 6.8$ cm^{-1}, and $Z'J' = -0.3$ cm^{-1} with $R = 3.66 \times 10^{-6}$ for complex **1**, $J = +39.0$ cm^{-1}, $g = 2.27$, $D = 7.3$ cm^{-1}, and $Z'J' = -0.19$ cm^{-1} with $R = 1.16 \times 10^{-4}$ for complex **4**, and $J = +6.2$ cm^{-1}, $g = 2.19$, $D = -0.22$ cm^{-1}, and $Z'J' = -1.6$ cm^{-1} with $R = 3.07 \times 10^{-5}$ for complex **3**. These values should be assumed with caution because the Ginsberg expression gives accurate values of J and g but parameters D and $Z'J'$ are not well determined from magnetic susceptibility data.[30,31]

The variable-temperature magnetic susceptibility data recorded for **2** are shown in Figure 6 in the form $\chi_M T$ vs T. From this, one can observe clearly that the Ni(II) atoms of the dinuclear unit show very weak coupling. The calculated J value, using the previous Ginsberg equation, does not exceed -2 cm^{-1} (very weak antiferromagnetic coupling). The best-fitting parameters obtained are $J = -1.85$ cm^{-1}, $g = 2.27$, $D = 0.07$ cm^{-1}, and $Z'J' = 0.24$ cm^{-1} with $R = 1.63 \times 10^{-4}$. The calculated J value is intermediate between the two dimers in the cell.

The difference in the magnitude and the sign of the magnetic exchange interactions found for **1**−**4** can be satisfactorily explained in terms of the kind of bridged ligand and the interaction between the metal centers and these ligands.

The Ni−O−Ni angles in **1**−**3** are large (>100°), suggesting that any exchange via phenolate bridge is unlikely to be ferromagnetic and might, in fact, be expected to mediate a weak antiferromagnetic contribution on the basis of the typical behavior of hydroxide[32] and alkoxide[33] bridged dinuclear copper(II) compounds and phenoxide-bridged dinuclear nickel(II) complexes,[34] this being the case for complexes **1**−**3**.

On the other hand, the azido ligand is ferromagnetic coupler when it bridges two metal ions through a $\mu_{1,1}$ fashion. Azides usually bridge via the two terminal nitrogen atoms ($\mu_{1,3}$-azido) or through only one of the terminal nitrogen atoms ($\mu_{1,1}$-azido). In the latter case, the coupling between the bridged paramagnetic metal ions is ferromagnetic for a wide range of M−N−M angles.[9]

As expected, complex **4** exhibits a strong ferromagnetic interaction ($J = +39.0$ cm^{-1}) that lies in the upper range of the interaction reported previously for dibridged azido Ni(II) in $\mu_{1,1}$ fashion.[35]

Complex **1** also exhibits a ferromagnetic interaction but with smaller magnitude than that found in complex **4** (+25.6 cm^{-1}), Table 6. This can be attributed to an effect similar to the anticomplementarity of the phenolate group, which exerts an antiferromagnetic contribution: the phenolate ligand reduces the expected strong ferromagnetic contribution of the azide bridge. As result, complex **1** shows a moderate ferromagnetic coupling as an average of both interactions through the azide and through the phenoxo ligands.

(29) Ginsberg, A. P. *Inorg. Chim. Acta Rev.* **1971**, *5*, 45.
(30) Duggan, M. D.; Barefield, E. K.; Hendrickson, D. N. *Inorg. Chem.* **1973**, *12*, 985.
(31) Battaglia, L. P.; Bianchi, A.; Bonamartini-Corradi, A.; Garcia-Espana, E.; Micheloni, M.; Julve, M. *Inorg. Chem.* **1988**, *27*, 4174.
(32) (a) Crawford, V. H.; Richardson, H. W.; Wasson, J. R.; Hodgson, D. J.; Hatfield, W. E. *Inorg. Chem.* **1976**, *15*, 2107. (b) Hodgson, D. J. *Prog. Inorg. Chem.* **1975**, *19*, 173. (c) Asokan, A.; Varghese, B.; Manoharan, P. T. *Inorg. Chem.* **1999**, *38*, 4393. (d) Charlot, M. F.; Jeannin, S.; Kahn, O.; Licrece-Abaul J.; Martin-Freere, J. *Inorg. Chem.* **1979**, *18*, 1675.
(33) (a) Handa, M.; Koga, N.; Kida, S. *Bull. Chem. Soc. Jpn.* **1988**, *61*, 3853. (b) Kodera, M.; Terasako, N.; Kita, T.; Tachi, Y.; Kano, K.; Yamazaki, M.; Koikawa, M.; Tokii, T. *Inorg. Chem.* **1997**, *36*, 3861.
(34) (a) Nanda, K. K.; Thompson, L. K.; Bridson, J. N.; Nag, K. *J. Chem. Soc., Chem. Commun*. **1994**, 1337. (b) Nanda, K. K.; Das, R.; Thompson, L. K.; Venkatsubramanian, K.; Paul, P.; Nag, K. *Inorg. Chem*. **1994**, *33*, 1188.
(35) Vicente, R.; Escuer, A.; Ribas, J.; El Fallah, M. S.; Solans, X.; Font-Bardia, M. *Inorg. Chem.* **1993**, *32*, 1920.

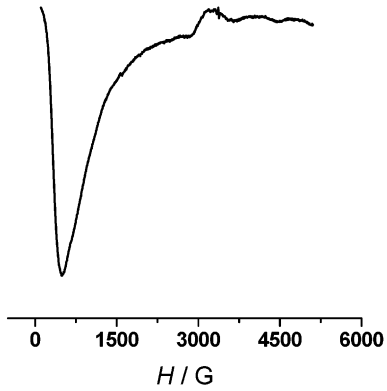

Figure 7. X-band EPR spectrum of a powdered sample of **1**, showing the ±2 transition at low field corresponding to the $S = 2$ anisotropic ground state.

Table 6. Selected Structural Parameters and Exchange Coupling for Complexes **1**−**4**

complex	Ni···Ni (Å)	Ni−O−Ni (deg)	Ni−N−Ni (deg)	J (cm^{-1})
1	3.187	106.8	96.2	+25.6
2A	3.328	110.5	96.6	−2
2B	3.344	112.4		
3	3.305	110.4	96.2	+6.2
4	3.286		102.5/99.4	+39.0

The cyanate ligand is also characterized with the same versatility as the azide ligand bridge, but under similar conditions, the magnitude of the interaction is usually smaller than observed in azide compounds.[36] Also, it is worth noticing that in compound **3** the bridging angle around the phenoxo oxygen is larger than in compound **1** (4° larger than in the azide compound). This yields a greater antiferromagnetic effect[34] but not sufficient to fully compensate the cyanate ferromagnetic effect, which may explain why the global ferromagnetic interaction takes over in **3** (+6.2 cm^{-1}).

In the case of complex **2**, a net antiferromagnetic coupling (very weak, $J = -2$ cm^{-1}) is observed. This may be a result of the interactions arising from the two different bridging groups: thiocyanate−phenolate in **2A** and acetate−phenolate in **2B**. It is well-known that thiocyanate usually propagates a weak ferromagnetic coupling[14,37] and acetate, with a *syn*−*syn* conformation, generally gives rise to an antiferromagnetic coupling,[38] thereby supporting our interpretation.

From the EPR measurements carried out on compounds **1**−**4**, it is of interest to note that in complex **1** the spectrum recorded at low temperature shows only one absorption at very low field (Figure 7). For an axial integer $S = 2$ spin system, the zero-field interaction (D parameter) splits the m_s levels into two doublets $m_s = |\pm 2\rangle$ and $|\pm 1\rangle$ and one $m_s = |0\rangle$ state. Transitions between these Kramer doublets are not possible due to the D value expected for the nickel(II) ion. For a rhombic distortion, the E parameter splits the $m_s = |\pm 2\rangle$ and $|\pm 1\rangle$ Kramer doublets giving a Δ_2 and Δ_1 gap at zero field. The Δ_1 increase is strongly dependent on E and is usually much greater than the $g\beta H$ energy of an X-band measurement. In contrast, the Δ_2 increase is a function of E^2/D and the ±2 transition usually lies in the low-field region of the spectra.[39] The expected spectra for an $S = 2$ system then consist of only one signal at very low field, which is in agreement with the experimental spectrum of **1**. This type of EPR spectrum is similar to previously reported manganese(III), iron(IV), and cobalt(II) spectra.[40−42]

Concluding Remarks

The Schiff base L[1] contains three or four separate binding subunits, each being able to coordinate one metal ion and the phenol group; in its deprotonated form, it has a strong tendency to bridge the two metal ions. For this reason, the two metal ions are forced to remain close to each other, and the phenolate group plays a key role in determining the molecular geometry of the binuclear species. Moreover, because of the number of binding sites, the ligand does not completely saturate the coordination sites of the metal ions and the complexes formed can be used to assemble at least one secondary ligand. This capability is well illustrated in the crystal structures obtained here using Ni(II) metal ions. In all cases the Ni···Ni bond distances were very close to each other.

The magnetic behavior of compounds **1**−**4** ranged from ferromagnetism to antiferromagnetism depending on the pseudohalide ligand which bridged the two nickel (II) atoms.

The EPR spectrum of complex **1** showed one absorption at very low field, typical of an axial integer $S = 2$ spin system.

Acknowledgment. A grant from the CSIR, New Delhi, India, to S.K.D. is gratefully acknowledged. The grant from the UGC, New Delhi, India, is also gratefully acknowledged. M.S.E.F. is grateful for a grant from the Ministerio de Ciencia y Tecnología (Programa Ramón y Cajal). This work was also supported by Grant BQU2000/0791 from the DGI (Direccion General de Investigación).

Supporting Information Available: X-ray crystallographic files, in CIF format, and a pdf file containing additional structural details for **1**−**4**. This material is available free of charge via the Internet at http://pubs.acs.org.

IC0352553

(36) (a) Mallah, T.; Khan, O.; Gouteron, J.; Jeannin, S.; Jeannin, Y.; O′Conner, J. *Inorg. Chem.* **1987**, *26*, 1375. (b) Khan, O.; Mallah, T.; Gouteron, J.; Jeannin, S.; Jeannin, Y. *J. Chem. Soc., Dalton Trans.* **1989**, 1117.
(37) Rojo, T.; Cortes, R.; Lezama, L.; Arriortua, M. I.; Urtiaga, K.; Willeneuve, G. *J. Chem. Soc., Dalton Trans.* **1991**, 1779.
(38) Fortea, A. R.; Alemany, P.; Alvarez, S.; Ruiz, E. *Chem.—Eur. J.* **2001**, *7*, 627.
(39) Abragam, A.; Bleaney, B. In *Electron Paramagnetic Resonance of Transition Ions*; Oxford University Press: New York, 1986; pp 209−216.
(40) Dexheimer, S. L.; Gohdes, J. W.; Chan, M. K.; Hagen, K. S.; Armstrong, W. H.; Klein, M. P. *J. Am. Chem. Soc.* **1989**, *111*, 8923.
(41) Kostka, K. L.; Fox, B. G.;. Hendrich, M. P.; Collins, T. J.; Rickard, C. E. F.; Wright, L. J.; Münch, E. *J. Am. Chem. Soc.* **1993**, *115*, 6746.
(42) Papaefstathiou, G. S.; Escuer, A.; Raptopoulou, C. P.; Terzis, A.; Perlepes, S. P.; Vicente, R. *Eur. J. Inorg. Chem.* **2001**, 1567.